Eur. Phys. J. B **42**, 345–350 (2004)
DOI: 10.1140/epjb/e2004-00389-0

THE EUROPEAN PHYSICAL JOURNAL B

Interaction between concentric tubes in DWCNTs

R. Pfeiffer[1,a], Ch. Kramberger[1,2], F. Simon[1], H. Kuzmany[1], V.N. Popov[3], and H. Kataura[4]

[1] Institut für Materialphysik, Universität Wien, Strudlhofgasse 4, 1090 Wien, Austria
[2] Leibniz Institute of Solid State and Materials Research Dresden, Helmholtzstrasse 20, 01069 Dresden, Germany
[3] Faculty of Physics, University of Sofia, Sofia, Bulgaria
[4] AIST, Central 4, Higashi 1-1-1, Tsukuba, 305-8562 Ibaraki, Japan

Received 14 June 2004 / Received in final form 15 September 2004
Published online 23 December 2004 –

Abstract. A detailed investigation of the Raman response of the inner tube radial breathing modes (RBMs) in double-wall carbon nanotubes is reported. It revealed that the number of observed RBMs is two to three times larger than the number of possible tubes in the studied frequency range. This unexpected increase in Raman lines is attributed to a splitting of the inner tube response. It originates from the possibility that one type of inner tubes may form in different types of outer tubes. In this case, a splitting of lines results since the inner tube RBM frequency depends on the diameter of the outer tube. Finally, a comparison of the inner tube RBMs and the RBMs of tubes in bundles gave clear evidence for a stronger interaction between tubes in a bundle as compared to the interaction between inner and outer tubes.

PACS. 81.07.De Nanotubes – 81.05.Tp Fullerenes and related materials – 78.30.Na Fullerenes and related materials

1 Introduction

Single-wall carbon nanotubes (SWCNTs) [1, 2] have attracted a lot of scientific interest over the last decade due to their unique structural and electronic properties. In 1998, Smith et al. [3] discovered that fullerenes can be encapsulated in SWCNTs, forming so-called peapods [4–6]. By annealing the peapods at high temperatures in a dynamic vacuum the enclosed C_{60} peas transform into SWCNTs within the outer tubes, thus producing double-wall carbon nanotubes (DWCNTs) [7, 8]. The growth process of the inner tubes is a new route for the formation of SWCNTs under shielded conditions in the absence of any additional catalyst.

A detailed Raman study of the radial breathing modes (RBMs) of the inner tubes revealed intrinsic linewidths down to $0.4\,\mathrm{cm}^{-1}$ [9]. These small linewidths indicate long phonon lifetimes and therefore highly defect free inner tubes. Thus, they are a direct experimental evidence for a nano-cleanroom reactor on the inside of SWCNTs.

Peapod grown DWCNTs are also interesting from another point of view. Usually, they are produced from standard SWCNTs with diameters around 1.4 nm. Taking into account the van der Waals interaction between the walls this means that the diameters of the inner shell tubes are around 0.7 nm. For these tubes the possible diameters can no longer be assumed to form a quasi-continuum. Additionally, due to the inverse relation between RBM frequency and diameter, the spectral distance between the RBMs of different inner tube types is (with few exceptions) much larger than between different outer tube RBMs. This opens the possibility to study the properties of individual SWCNTs in a bulk sample. A first application of this was the assignment of the chiral vectors to all inner tubes [10].

Studying the Raman response of the inner tube RBMs in high resolution at 20 K revealed that the number of observed lines is about two to three times larger than the number of geometrically allowed inner tubes. In the following, we show that this unexpected increase of Raman lines can be attributed to a splitting of the response from the inner tubes. This splitting originates from the possibility for one inner tube type to form in several outer tube types (with different diameters) and the fact that the RBM frequency of the inner tube depends on the diameter of the encapsulating parent tube. A quantitative explanation for the splitting was obtained by calculating the RBM frequencies of the inner tubes as a function of the outer tube diameter within a continuum model. Using two different scenarios regarding the possible inner-outer shell pairs, we compared the splitting obtained from the simulation with the experimentally obtained splitting. From this we conclude that not only the best fitting inner tubes are formed.

2 Experimental

The starting material for the DWCNTs were C_{60} peapods (in the form of bucky paper), produced by a previously described method [5]. The mean diameter of the assumed Gaussian diameter distribution of the outer tubes was 1.39(2) nm with a variance of 0.1 nm, as determined from

[a] e-mail: rpfei@ap.univie.ac.at

the RBM Raman response [11]. The filling of the tubes large enough for C_{60} to enter was close to 100% as evaluated from a Raman [12] and EELS analysis [13]. These peapods were slowly heated up to 1280 °C in a dynamic vacuum, annealed for 2 h, and were then slowly cooled down to room temperature.

To compare the RBM positions of the inner tubes with that of the same tube types in a bundle, we recorded also the Raman response of a bulk SWCNT sample produced with the high-pressure carbon monoxide (HiPco) scheme [14]. HiPco tubes have a broad diameter distribution from 0.8 to 1.4 nm, centered around 1.0 nm [15].

The Raman spectra were measured with a Dilor xy triple spectrometer using various lines of an Ar/Kr laser, a He/Ne laser and a Ti:sapphire laser. The spectra were recorded at 90 and 20 K in normal (NR) and high resolution (HR) mode, respectively ($\Delta\bar{\nu}_{\rm NR} = 1.3\,{\rm cm}^{-1}$ and $\Delta\bar{\nu}_{\rm HR} = 0.4\,{\rm cm}^{-1}$ in the red). In these measurements the samples were glued on a copper cold finger with silver paste.

3 Theory

The RBM frequencies of a given DWCNT were calculated using a continuum model (model 2 in Ref. [16]). In this model, the DWCNT is represented by two nested hollow cylinders with diameters $d_{\rm i}$ and $d_{\rm o}$ of the inner and outer shells, respectively. The interaction between two points at a distance r on different shells was described by a Lennard-Jones (LJ) potential

$$V(r) = 4\epsilon[(\sigma/r)^{12} - (\sigma/r)^6]\,, \qquad (1)$$

where $\epsilon = 2.964\,{\rm meV}$ and $\sigma = 0.3407\,{\rm nm}$ [17].

The total interaction energy Φ between the two shells was calculated by a numerical integration over a unit length of the shells. For this, the two shells were approximated by quadratic meshes. The mass of the carbon atoms was equally distributed over the meshes and located in their centers. The interaction energy was then calculated by summing the LJ potential over all mesh centers. The size of the meshes was reduced until the interaction energy had converged.

The interaction part of the dynamical matrix was then obtained by a numerical differentiation of Φ with respect to $d_{\rm i}$ and $d_{\rm o}$. It was also assumed that the separate shells are elastic and are characterized with force constants $k_{\rm i}$ and $k_{\rm o}$ for the radial breathing motion. The k's were determined from the RBM frequency $\bar{\nu}_{\rm RBM}$ of a tube which is related to the tube diameter d by [18–20]

$$\bar{\nu}_{\rm RBM} = C_1/d + C_2\,, \qquad (2)$$

where C_1 and C_2 are constants. The role of C_2 is to account for all frequency shifts due to the interaction with the environment. Since this interaction was explicitly modeled in our simulations, C_2 was set zero in the calculations. The shell diameters were taken from a DFT study [10], giving

$$d = \left(\frac{1}{d_{\rm G}} - \frac{0.0050}{d_{\rm G}^2} - \frac{0.0013}{d_{\rm G}^4}\right)^{-1}, \qquad (3)$$

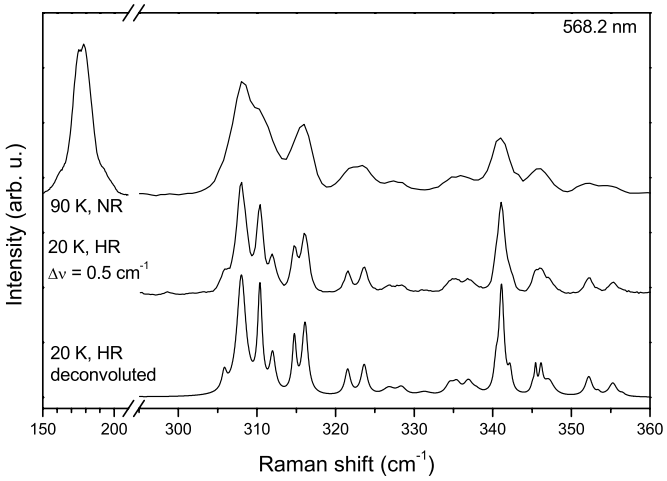

Fig. 1. RBM Raman response of the inner tubes at 90 K and normal resolution, 20 K and high resolution, and Lorentzian components of the 20 K and high resolution spectrum (top to bottom).

where

$$d_{\rm G} = \frac{\sqrt{3}\,a_{\rm CC}}{\pi}\sqrt{m^2 + mn + n^2} \qquad (4)$$

is the graphene folding diameter, $a_{\rm CC} = 0.141\,{\rm nm}$ is the C−C distance in graphene and (m, n) is the chiral vector of the tube. Especially for small diameter tubes ($d \lessapprox 1\,{\rm nm}$) the DFT derived diameter has to be used instead of the graphene folding diameter.

The dynamical matrix D of the DWCNT can then be written in the form

$$D = -\frac{1}{\sqrt{m_{\rm i} m_{\rm o}}}\begin{pmatrix} k_{\rm i} + \partial^2\Phi/\partial d_{\rm i}^2 & \partial^2\Phi/\partial d_{\rm i}\partial d_{\rm o} \\ \partial^2\Phi/\partial d_{\rm o}\partial d_{\rm i} & k_{\rm o} + \partial^2\Phi/\partial d_{\rm o}^2 \end{pmatrix}, \qquad (5)$$

where $m_{\rm i}$ and $m_{\rm o}$ are the masses (per unit length) of the inner and outer shells, respectively. We note in passing that this form of D differs from that in reference [21], where the partial derivatives were assumed to be equal. The RBM frequencies are finally obtained as solutions of the vibrational eigenvalue problem for the DWCNT.

The results of the relaxation of the DWCNTs with respect to a displacement of the shell axis from the coaxial position revealed that the two shells remain concentric for $\Delta d = d_{\rm o} - d_{\rm i} < 0.78\,{\rm nm}$. For diameter differences $\Delta d > 0.78\,{\rm nm}$ the inner tube moved away from the coaxial position. For coaxial shells, the relaxation of the DWCNT with respect to $d_{\rm i}$ (for fixed $d_{\rm o}$) or vise versa yielded an equilibrium value for Δd of about 0.68 nm.

For the following analysis, we calculated the RBM frequencies for all inner-outer tube pairs with inner tubes between $(5, 3)$ ($d_{\rm i} = 0.55\,{\rm nm}$) and $(14, 0)$ ($d_{\rm i} = 1.09\,{\rm nm}$) and possible diameter differences in the range 0.66−0.74 nm.

4 Experimental results

Figure 1 depicts the Raman response of the inner tube RBMs. While the NR spectrum shows only very broad lines, the HR spectrum reveals much richer details with

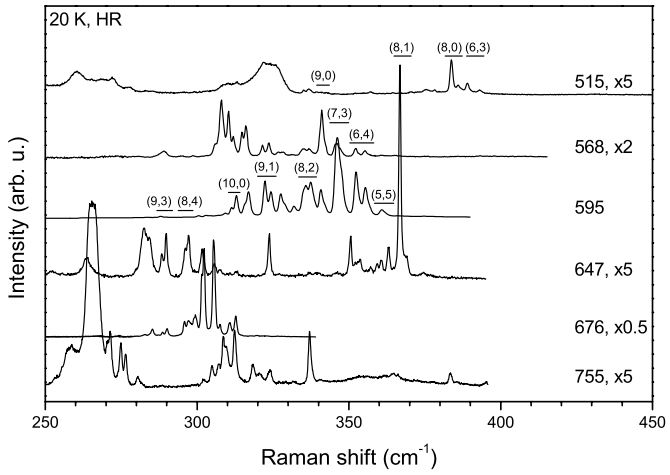

Fig. 2. High resolution Raman response of the inner tube RBMs for several excitation wavelengths at 20 K. Selected chiralities after reference [10]. Split widths are indicated by lines under the chirality vectors.

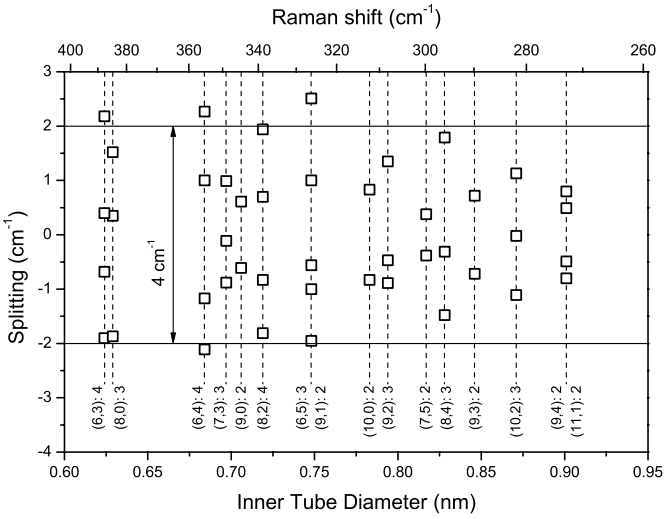

Fig. 3. Number of split components and width of splitting for selected individual inner tubes from the spectra in Figure 2 after subtracting the mean value of the RBM frequencies. The dashed lines connect split components assigned to the same inner tube. Additionally, the tube chiralities and the number of split components is included.

rather small linewidths. This becomes even more obvious when the as measured spectrum was fitted with Voigtian lines (Lorentzians convoluted with a Gaussian spectrometer response) where the spectrometer response was taken from a fit to the elastically scattered light. The resulting Lorentzian components are equivalent to a deconvoluted spectrum [9].

Using the diameter-frequency relationship from equation (2) it is possible to determine the number of inner tubes for a given frequency range. There is some ongoing discussion on the value of C_1, where reported numbers range from 224 to 250 $\mathrm{cm}^{-1}\,\mathrm{nm}$ [10, 22, 23]. In the following, we use the value of 233 $\mathrm{cm}^{-1}\,\mathrm{nm}$ as derived from a systematic analysis of the inner shell tubes in DWCNTs [10].

Regardless of the exact value of C_1, between 300 and 350 cm^{-1} one should only see the response of eight different tubes. By looking at the HR spectrum in Figure 1, one can easily identify about 18 peaks and shoulders in this range. Hence, one can observe about two to three times more RBMs as there are geometrically allowed tubes.

Figure 2 depicts selected high resolution Raman spectra of the inner RBMs. Using the refined frequency-diameter relation from reference [10], one should find the RBMs of 28 distinct inner tubes between 270 and 400 cm^{-1}. Again the observed number of lines in this region is about three times larger. For some chiralities the split widths are indicated by lines under the folding vector components.

In order to determine the number of the split components and the width of the splitting, we fitted the spectra from Figure 2 with a number of Voigtian lines. Using the chirality assignment of reference [10], sets of RBM frequencies were assigned to selected inner tube types. The tubes were selected such that the assignment was unambiguous. If the frequency sets of two inner tubes overlapped the tubes were not considered in the following analysis.

For the selected inner tubes, we subtracted the mean value from the assigned frequencies and plotted the split components vs. inner tube diameter in Figure 3. It shows that the number of split components ranges between two and four with no obvious influence of the tube chirality. Additionally, the width of the splitting is about 4 cm^{-1}. Since not all inner tubes were considered in the analysis, this splitting value is a lower limit.

5 Simulation results

Figure 4 (top) demonstrates the dependence of the calculated RBM frequency of a $(6, 4)$ inner tube on the diameter of the outer tube. The isolated $(6, 4)$ tube has a diameter of $d_\mathrm{i} = 0.686\,\mathrm{nm}$ and a frequency of $\bar{\nu}^{\mathrm{isolated}}_{\mathrm{inner\ RBM}} = 339.8\,\mathrm{cm}^{-1}$ (excluding C_2) [10]. Due to the interaction between the two shells, the inner RBM frequency increases by up to 12 cm^{-1} with decreasing outer tube diameter. In the diameter difference range studied, the RBM frequencies can be fitted with $(a/\Delta d)^b + \bar{\nu}^{\mathrm{isolated}}_{\mathrm{RBM}}$ (see Fig. 4, lower left corners).

Similarly, Figure 4 (bottom) depicts the RBM frequency of a $(10, 10)$ outer tube as a function of the inner tube diameter. Again, the larger the inner tube diameter the larger the shift of the outer tube RBM. Indeed, slight upshifts of a few cm^{-1} of the outer tube RBMs of DWCNTs were observed when directly compared with the empty reference SWCNTs. However, due to the quasi-continuous diameter distribution of the outer tubes, exact measurements are difficult.

In a first step, we assumed that in all outer tubes in our sample only the best fitting inner tubes are formed. Best fitting means that for every outer tube the inner tube was selected such that $|d_\mathrm{o} - d_\mathrm{i} - 0.68\,\mathrm{nm}|$ becomes a minimum. The splitting calculated for this assumption is depicted in Figure 5 (top). The number of split components and the width of the splitting are smaller than the experimentally observed values. Therefore, in a second step, we

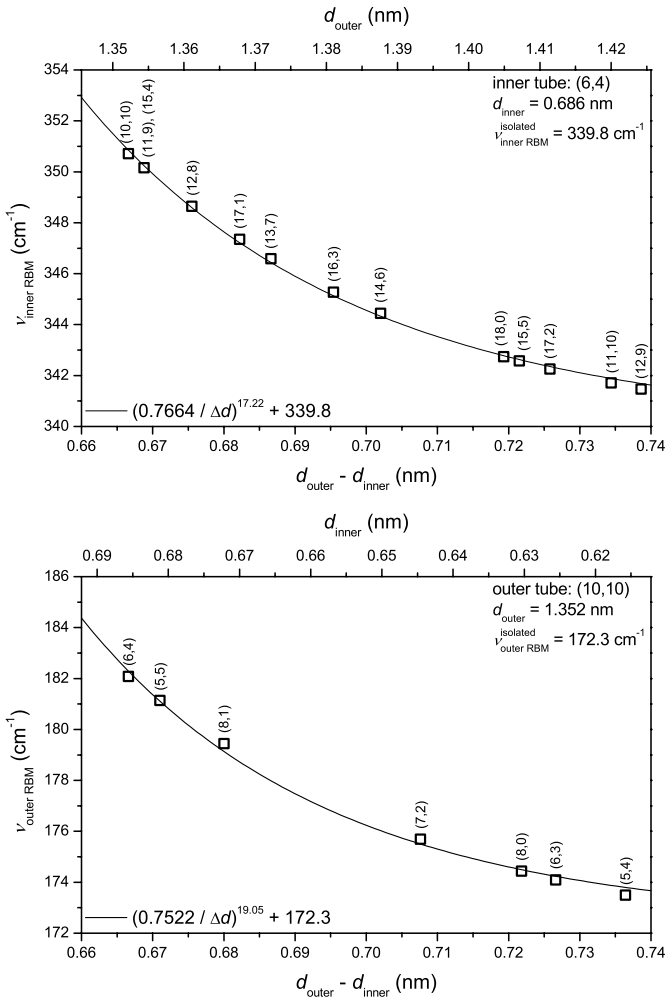

Fig. 4. Top: Calculated RBM frequency of a $(6,4)$ inner tube as a function of the encapsulating tube diameter d_o. Bottom: Calculated RBM frequency of a $(10,10)$ outer tube as a function of the encapsulated tube diameter d_i. The diameters were calculated from equation (3). The lines are fits with the given parameters as indicated in the lower left corners.

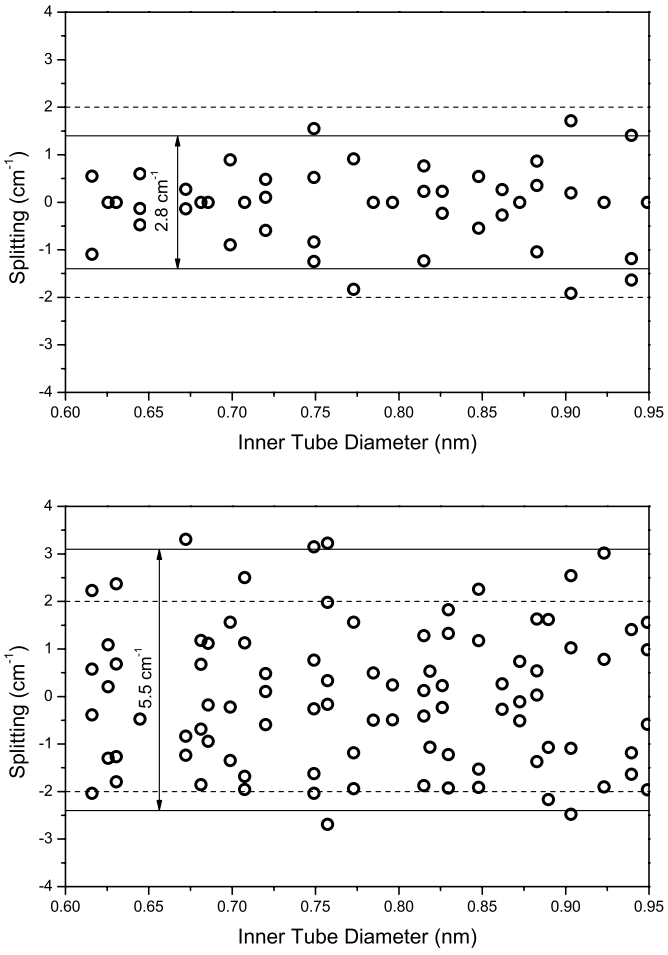

Fig. 5. Number of split components and width of splitting for individual inner tubes from the theory after subtracting the mean value of the calculated RBM frequencies. Top: Only the best fitting inner tubes are formed. Bottom: The best and second best fitting inner tubes are formed. The dashed lines mark the width of splitting obtained from the experiment.

assumed also the second best fitting inner tubes to form. As Figure 5 (bottom) shows, this assumption results in a splitting of $5.5\,\mathrm{cm}^{-1}$ which is larger than observed. This suggests that also second best fitting inner tubes form in cases where the energy balance is in favor for it.

Figure 6 compares the percentages of the number of inner tube split components obtained from the experiment with the two theoretical models discussed above. If only best fitting inner tubes form, mainly 1, 2, and 3 split components should be observed. If best and second best fitting inner tubes form, mainly 3 and 4 split components are to be expected. The experimental curve lies between the two model curves peaking around 2−3 split components.

6 Comparison with tubes in bundles

Our calculations have shown that the upshift of the inner tube RBMs can be as high as $12\,\mathrm{cm}^{-1}$. Such an upshift of

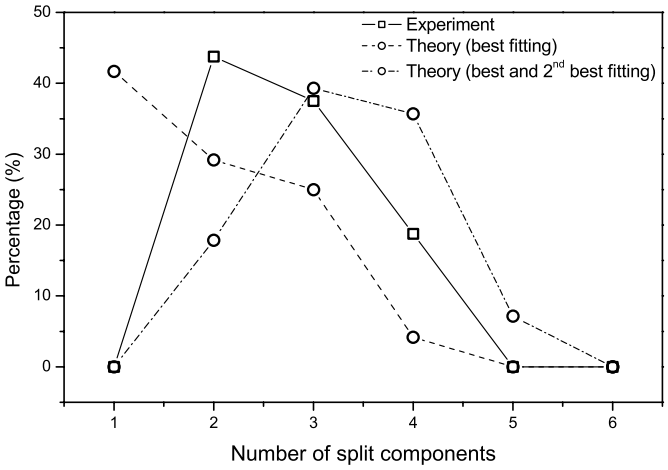

Fig. 6. Percentages of the number of split components from the experiment and the two theoretical models.

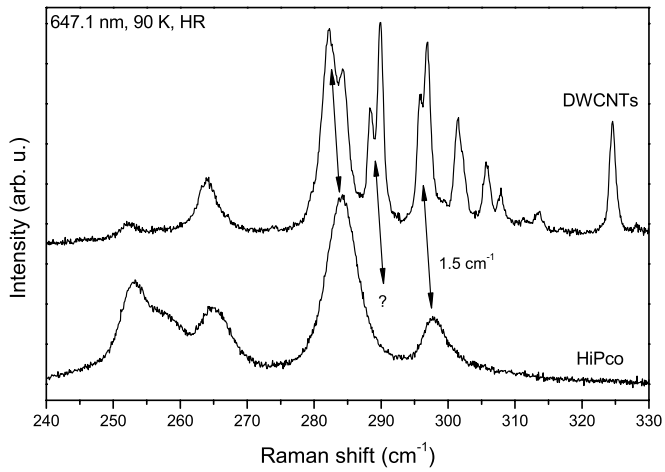

Fig. 7. RBM Raman response of small diameter tubes as inner tubes of DWCNTs (top) and in a typical HiPco sample (bottom). The HiPco RBMs are $1.5\,\mathrm{cm}^{-1}$ more upshifted than the inner tube RBMs. Additionally, the resonances of some bundled tubes are different to the corresponding encaged tubes.

the RBM frequency does not only occur for inner tubes in DWCNTs but also for SWCNTs in bundles [20, 24]. In both cases this shift is due to the van der Waals interaction with the surrounding tubes. However, in the case of the concentric tubes the interaction is between a tube outside and a tube inside whereas in the case of the bundles it is between two tube outsides. Therefore, it was interesting to compare the upshift of encaged and bundled tubes. For this comparison we used a typical HiPco sample with a broad diameter distribution such that similar tube diameters could be compared.

Figure 7 depicts the RBM Raman response of the inner tubes and the HiPco tubes. The two samples were measured simultaneously in the same experiment. This means, the spectra were recorded without changing the spectrometer position which guarantees a high precision of the measured frequency differences. Several observations can be made in this figure. First, compared to the inner tube RBMs the HiPco RBMs are broader and do not get narrower in the HR mode. This is an important detail of the results, since it demonstrates that the narrow linewidth is not a mere consequence of the small tube diameter. It rather underlines the high quality of the inner tubes. Additionally, the HiPco RBMs may be broadened due to the inhomogeneous environment within the bundles [24].

Second, the HiPco RBMs are about $1.5\,\mathrm{cm}^{-1}$ more upshifted than the inner tube RBMs. The stronger upshift of the RBMs of the HiPco sample suggests a stronger interaction between the tubes in the bundles as compared to the interaction between the inner and outer shells of a DWCNT. This experimental evidence is rather surprising, since the interaction area for one tube in a bundle is certainly smaller than for inner-outer tube pairs. Thus, the reason for the upshift is not yet fully understood. It may be related to a larger equilibrium diameter difference in the concentric tubes as compared to the distance between tubes in the bundles. This increased distance would reduce the interaction between inner and outer tubes. There is some support for this idea from the fact that the experimentally observed wall to wall distance in the concentric tubes is slightly larger than the value expected from graphite (0.72 compared to 0.68 nm) [25]. Since the wall to wall distance enters with a high power into the interaction potential a reduced interaction is reasonable. Additionally, the inhomogenous and non-radially symmetric environment in the bundles may also play a role.

Third, some RBMs are missing in the HiPco spectrum (in this case the $(9, 3)$ tube). Since the RBM response of even thinner tubes than the missing species is present in the HiPco spectrum the observed absence cannot be explained by the diameter distribution of the HiPco material. In fact, the missing lines show up for other excitation energies [26]. This means, the resonances of the encaged tubes are slightly different to the resonances in the bundled tubes. This change in resonance energy can depend on the tube chirality. In fact, a chirality dependence of the electron-lattice interaction was recently reported from ab initio calculations [27].

7 Discussion

The continuum model we are using was parameterized for graphite [17] and subsequently used for simulations of multi-shell fullerenes [28] and multi-wall carbon nanotubes [16]. As mentioned above, it resulted in an equilibrium diameter difference of about 0.68 nm. Abe et al. [25] reported X-ray measurements that suggest a more likely diameter difference of 0.72 nm. Even though a recent Raman analysis supports this value [29], we think our main results are not affected by this difference. For larger equilibrium diameters the interaction will be weaker in general and therefore more likely reduce the calculated splitting.

In the simulations we were using, only the diameter dependence of the RBM frequency shift can be evaluated but not the influence of differing chiralities of the inner and outer tubes in one DWCNT. Due to the large unit cells of the DWCNTs such microscopic calculations would be very difficult. Only special geometries such as $(5, 5)@(10, 10)$ can be evaluated. Additionally, the LJ simulations are based on the approximation of the atoms with point charges. In practice, the interaction between the two layers arises from a quantum mechanical interaction between the delocalized electron density of these layers thus making the stacking less important. Furthermore, our simplification is justified by the experimental results depicted in Figure 3 which show no obvious dependence of the number of split components on the chiral angle of the inner tube. Therefore, we conclude that the chirality plays only a minor role. On the other hand, an influence of the chirality on the interaction energy may not be completely negligible. It can be the reason for the observed best and second best fitting tube grown inside the outer tube.

The good consistency between the calculated splitting and the observed results further supports the given interpretation. With these results each component of the split lines can be assigned to a distinct double-wall pair.

Accepting the radial tube-tube interaction as the reason for the extended splitting has also important consequences for the growth dynamics. Always those tubes will grow which are energetically most favorable at the high transformation temperatures. This holds even if nucleation of inner tube growth starts at different positions in the outer tube. In our understanding, the energetically more favorable tubes will eventually "eat up" the less favorable ones. Interesting configurations occur for the growth of a chiral tube inside an achiral tube. There, the two possible stereo-isomers are equal in energy but cannot match. The proven low concentration of defects on the inner tubes evidences that always one of the equienergetic tubes will win.

8 Summary

We have shown that the RBMs of the inner tubes of DWCNTs are split into several components and provided a quantitative understanding from calculations. The splitting is attributed to the interaction between inner and outer tubes that causes a change of the inner tube RBM frequency. Since it is possible that one type of inner tube forms in several types of outer tubes (with slightly different diameters) every inner tube gives rise to more than one RBM in the Raman spectrum. We have further demonstrated that not only the best fitting structure is established. Finally, we have compared the RBM Raman response of inner tubes with that of similar diameter tubes in bundles. Surprisingly, the bundled tube RBMs are more upshifted than the encaged tube RBMs and some Raman lines are missing in the HiPco spectra. The latter effect is considered as a consequence of a chirality dependent shift of resonance levels.

The authors acknowledge financial support from the FWF in Austria, project P14893, and from the EU Marie-Curie project MEIF-CT-2003-501099 (PATONN). VNP was supported by a fellowship from the Federal Science Policy Office for promoting the S&T cooperation with Central and Eastern Europe, by a NATO CLG, and from the EU Marie-Curie project MEIF-CT-2003-501080.

References

1. S. Iijima, T. Ichihashi, Nature **363**, 603 (1993)
2. A. Thess, R. Lee, P. Nikolaev, H. Dai, P. Petit, J. Robert, C. Xu, Y.H. Lee, S.G. Kim, A.G. Rinzler et al., Science **273**, 483 (1996)
3. B.W. Smith, M. Monthioux, D.E. Luzzi, Nature **396**, 323 (1998)
4. B.W. Smith, D.E. Luzzi, Chem. Phys. Lett. **321**, 169 (2000)
5. H. Kataura, Y. Maniwa, T. Kodama, K. Kikuchi, K. Hirahara, K. Suenaga, S. Iijima, S. Suzuki, Y. Achiba, W. Krätschmer, Synthetic Met. **121**, 1195 (2001)
6. F. Simon, H. Kuzmany, H. Rauf, T. Pichler, J. Bernardi, H. Peterlik, L. Korecz, F. Fülöp, A. Jánossy, Chem. Phys. Lett. **383**, 362 (2003)
7. S. Bandow, M. Takizawa, K. Hirahara, M. Yudasaka, S. Iijima, Chem. Phys. Lett. **337**, 48 (2001)
8. S. Bandow, G. Chen, G.U. Sumanasekera, R. Gupta, M. Yudasaka, S. Iijima, P.C. Eklund, Phys. Rev. B **66**, 075416 (2002)
9. R. Pfeiffer, H. Kuzmany, C. Kramberger, C. Schaman, T. Pichler, H. Kataura, Y. Achiba, J. Kürti, V. Zólyomi, Phys. Rev. Lett. **90**, 225501 (2003)
10. C. Kramberger, R. Pfeiffer, H. Kuzmany, V. Zólyomi, J. Kürti, Phys. Rev. B **68**, 235404 (2003)
11. H. Kuzmany, W. Plank, M. Hulman, C. Kramberger, A. Grüneis, T. Pichler, H. Peterlik, H. Kataura, Y. Achiba, Eur. Phys. J. B **22**, 307 (2001)
12. H. Kuzmany, R. Pfeiffer, C. Kramberger, T. Pichler, X. Liu, M. Knupfer, J. Fink, H. Kataura, Y. Achiba, B.W. Smith et al., Appl. Phys. A **76**, 449 (2003)
13. X. Liu, T. Pichler, M. Knupfer, M.S. Golden, J. Fink, H. Kataura, Y. Achiba, K. Hirahara, S. Iijima, Phys. Rev. B **65**, 045419 (2002)
14. J.H. Hafner, M.J. Bronikowski, B.R. Azamian, P. Nikolaev, A.G. Rinzler, D.T. Colbert, K.A. Smith, R.E. Smalley, Chem. Phys. Lett. **296**, 195 (1998)
15. P. Nikolaev, M.J. Bronikowski, R.K. Bradley, F. Rohmund, D.T. Colbert, K.A. Smith, R.E. Smalley, Chem. Phys. Lett. **313**, 91 (1999)
16. V.N. Popov, L. Henrard, Phys. Rev. B **65**, 235415 (2002)
17. J.P. Lu, X.-P. Li, R.M. Martin, Phys. Rev. Lett. **68**, 1551 (1992)
18. R.A. Jishi, L. Venkataraman, M.S. Dresselhaus, G. Dresselhaus, Chem. Phys. Lett. **209**, 77 (1993)
19. J. Kürti, G. Kresse, H. Kuzmany, Phys. Rev. B **58**, R8869 (1998)
20. L. Henrard, E. Hernández, P. Bernier, A. Rubio, Phys. Rev. B **60**, R8521 (1999)
21. E. Dobardžić, J. Maultzsch, I. Milošević, C. Thomsen, M. Damnjanović, Phys. Stat. Sol. (b) **237**, R7 (2003)
22. A. Jorio, R. Saito, J.H. Hafner, C.M. Lieber, M. Hunter, T. McClure, G. Dresselhaus, M.S. Dresselhaus, Phys. Rev. Lett. **86**, 1118 (2001)
23. S.M. Bachilo, M.S. Strano, C. Kittrell, R.H. Hauge, R.E. Smalley, R.B. Weisman, Science **298**, 2361 (2002)
24. L. Henrard, V.N. Popov, A. Rubio, Phys. Rev. B **64**, 205403 (2001)
25. M. Abe, H. Kataura, H. Kira, T. Kodama, S. Suzuki, Y. Achiba, K.-I. Kato, M. Takata, A. Fujiwara, K. Matsuda et al., Phys. Rev. B **68**, 041405(R) (2003)
26. F. Simon, R. Pfeiffer, C. Kramberger, M. Holzweber, H. Kuzmany, *The Raman response of double wall carbon nanotubes*, `arXiv:physics.cond-mat/0404110` (2004)
27. M. Machón, S. Reich, J. Maultzsch, P. Ordejón, C. Thomsen, in *Proceedings of the IWPEPNM* (2004), pp. 381–384
28. J.P. Lu, W. Yang, Phys. Rev. B **49**, 11421 (1994)
29. F. Simon, A. Kukovecz, C. Kramberger, R. Pfeiffer, F. Hasi, H. Kuzmany, H. Kataura, *Diameter selective characterization of single-wall carbon nanotubes*, `arXiv:physics.cond-mat/0403179` (2004)